Journal of Nuclear Materials 442 (2013) 195–207

Contents lists available at ScienceDirect

Journal of Nuclear Materials

journal homepage: www.elsevier.com/locate/jnucmat

Solubility properties of synthetic and natural meta-torbernite

Fanny Cretaz [a], Stéphanie Szenknect [a,*], Nicolas Clavier [a], Pierre Vitorge [b], Adel Mesbah [a], Michael Descostes [c], Christophe Poinssot [d], Nicolas Dacheux [a]

[a] ICSM UMR 5257 CNRS/CEA/UM2/ENCSM, Site de Marcoule – Bât 426, BP 17171, 30207 Bagnols/Cèze, France
[b] CEA, Nuclear Energy Division, DPC/SECR, Site de Saclay, Bât 391, 91191 Gif-sur-Yvette, France
[c] AREVA Mines/DEXP/DR&D-projet Envir@Mines, La Défense, 92084 Paris, France
[d] CEA, Nuclear Energy Division, DRCP/DIR, CEA Marcoule – Bât 400, BP 17171, 30207 Bagnols/Cèze, France

HIGHLIGHTS

- Solubility of synthesized meta-torbernite $(H_3O)_{0.4}Cu_{0.8}(UO_2)_2(PO_4)_2\cdot 7.6H_2O$.
- Solubility constant and thermodynamic data of formation were determined.
- Comparison with a natural sample: same steady state reached for both samples.
- Simulations performed under environmentally relevant conditions using the thermodynamic data obtained.

GRAPHICAL ABSTRACT

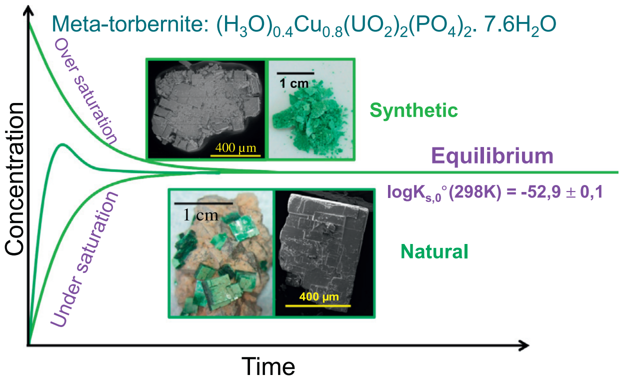

ARTICLE INFO

Article history:
Received 22 April 2013
Accepted 17 August 2013
Available online 2 September 2013

ABSTRACT

Meta-torbernite, $Cu(UO_2)_2(PO_4)_2\cdot 8H_2O$, is one of the most common secondary minerals resulting from the alteration of pitchblende. The determination of the thermodynamic data associated to this phase appears to be a crucial step toward the understanding the origin of uranium deposits or to forecast the fate and transport of uranium in natural media. A parallel approach based on the study of both synthetic and natural samples of meta-torbernite $(H_3O)_{0.4}Cu_{0.8}(UO_2)_2(PO_4)_2\cdot 7.6H_2O$ was set up to evaluate its solubility constant. The two solids were first thoroughly characterized and compared by means of XRD, SEM, X-EDS analyses, Raman spectroscopy and BET measurements. The solubility constant was then determined in both under- and supersaturated conditions: the obtained value appeared close to $\log K^{\circ}_{s,0}(298\ K) = -52.9 \pm 0.1$ whatever the type of experiment and the sample considered. The joint determination of Gibbs free energy ($\Delta_R G^{\circ}(298\ K) = 300 \pm 2\ kJ\ mol^{-1}$) then allowed the calculation of $\Delta_R H^{\circ}(298\ K) = 40 \pm 3\ kJ\ mol^{-1}$ and $\Delta_R S^{\circ}(298\ K) = -879 \pm 7\ J\ mol^{-1}\ K^{-1}$. From these values, the thermodynamic data associated with the formation of meta-torbernite $(H_3O)_{0.4}Cu_{0.8}(UO_2)_2(PO_4)_2\cdot 7.6H_2O$ were also evaluated and found to be consistent with those previously obtained by calorimetry, showing the reliability of the method developed in this work. Finally, the obtained data were implemented in a calculation code to determine the conditions of meta-torbernite formation in environmental conditions typical of a former mining site.

---

* Corresponding author.
E-mail address: stephanie.szenknect@cea.fr (S. Szenknect).

http://dx.doi.org/10.1016/j.jnucmat.2013.08.037

1. Introduction

Due to their extremely low solubilities under circumneutral pH conditions and phosphorous ubiquity in natural waters, uranyl phosphates are important phases for the control of uranium mobility in many oxidizing environments [1]. Subsurface application of polyphosphates is even considered as a promising remediation technology for uranium decontamination of the groundwater. Uranyl phosphates are encountered in a variety of altered uranium deposits [2]. With the development of the nuclear industry, the need for new economically exploitable uranium ore deposits also led to consider uranyl phosphates as potential phases of interest [3]. A major focus is now devoted to the uranium extraction from rock phosphate as sustainable secondary source for uranium. Indeed, such deposits contain millions of tons of uranium which may be extracted as a by-product of making fertilizers (see [4]), where the main minerals in the phosphate rock are apatite and fluorapatite. Another phosphate bearing mineral of interest is the meta-torbernite $Cu(UO_2)_2(PO_4)_2{\cdot}8H_2O$. While less common, such mineral frequently occurs in conjunction with other uranium minerals, as well as host rock minerals. It is often associated with conventional deposits of pitchblende/coffinite type as supergene alteration product ([5–9]).

This mineral may also play a key role in the migration of U in the framework of the deep geological repository of nuclear spent fuel. In Finland and Sweden, spent nuclear fuel is packed in copper canisters ([10,11]). The oxidative alteration of the UO_2 spent fuel matrix in the presence of copper could arise to torbernite-like phases.

Therefore, understanding the origin of uranium deposits or modeling the fate and transport of uranium in natural or contaminated settings require reliable solubility measurements or thermodynamic properties from which solubility can be calculated.

Despite the important role of this phase, rigorously constrained thermodynamic data are lacking. None of the published solubility constants of meta-torbernite were validated by the NEA Thermochemical Database Project, OECD–NEA-TDB [12]. Indeed, the previously reported values of solubility constants are not consistent and vary depending on the experimental conditions ($-33 < \log K^{\circ}_{s,0} < -53$) or have not been evaluated by NEA yet (publications subsequent to 2003). Vochten and Piret [7], Pekarek et al. [13], and Karyakin et al. [14] conducted their studies on synthetic (i.e. pure) samples at low pH without any extrapolation to standard conditions in order to determine the $K^{\circ}_{s,0}$ value. Ilton et al. performed solubility experiments in under- and supersaturation conditions on natural meta-torbernite crystals in nitric and phosphoric acids [15]. They used the Pitzer's formula to calculate the activities of the relevant species. Comparison of the solubility constant obtained by Ilton et al. ($\log K^{\circ}_{s,0} = -52.7 \pm 0.1$) with a value determined on a synthetic sample is thus necessary to conclude. In addition, Karyakin et al. [14] are the first who proposed values of standard enthalpy, standard Gibbs free energy and standard entropy of formation of meta-torbernite, using calorimetry. To our knowledge, these data were not confirmed in the literature for the corresponding dissolution reaction even though these parameters are needed to predict the possible formation and the solubility of meta-torbernite under relevant environmental conditions.

In this study, dissolution tests were performed in nitric, sulfuric, and hydrochloric media on both synthetic and natural samples of meta-torbernite. Thermodynamic equilibrium was also approached by the supersaturation method during the precipitation of pure meta-torbernite. The objectives were to obtain a reliable solubility product for meta-torbernite, to examine the nature of dissolution with varying solution compositions and then to compare the behavior of synthetic (pure) and natural minerals. Once the solubility constant was obtained, its variation versus temperature was used to determine the main thermodynamic functions associated with the dissolution reaction, $\Delta_R X^{\circ}$, or with the formation of meta-torbernite $\Delta_f X^{\circ}$ (where $X = H$, G and S).

2. Materials and methods

2.1. Synthesis

All the acid solutions used for the synthesis, dissolution and precipitation tests (H_3PO_4, HNO_3, HCl and H_2SO_4) were prepared from analytical grade reagents (supplied by Sigma or Fisher). The uranyl nitrate solution was prepared from metallic uranium. Uranium chips were dissolved in a solution of 6 mol L^{-1} HCl and the solution was then concentrated to obtain a final 2×10^{-1} mol L^{-1} solution of U(IV) [16]. Addition of H_2O_2 (9.8 mol L^{-1}) allowed quantitative oxidation of U(IV) to U(VI) then the precipitation of the studtite $UO_2(O_2)(H_2O)_2{\cdot}2H_2O$ [17]. The solid was separated from the supernatant by centrifugation (4 min, 4500 rpm), then washed with distilled water and dissolved in a 4 mol L^{-1} HNO_3 solution. The resulting solution was then heated to dry: an orange solid was obtained. Solution of uranyl nitrate used was obtained by dissolving the solid in solution of 5×10^{-2} mol L^{-1} HNO_3. Its final concentration was determined by inductively coupled plasma atomic emission spectrometry (ICP-AES) and α-liquid scintillation (PERALS, Photon Electron Rejecting Alpha Liquid Scintillation [18]).

The protocol used for the preparation of meta-torbernite was inspired by that previously reported by Berman [19]. It was based on the direct precipitation of a mixture of 85 mL of uranyl nitrate (pH = 1.1, $C_U = 2 \times 10^{-1}$ mol L^{-1}), 1.46 g of copper dichloride dihydrate with 8.5 mL of 2 mol L^{-1} H_3PO_4 at 333 K. After three days of maturation, the obtained green precipitate was separated from the supernatant by centrifugation (4 min, 4500 rpm), washed with distilled water then dried at 313 K in an oven. Precipitation yields exceeded 85%.

The natural meta-torbernite came from the Margabal mine at Entraygues-sur-Truyère (France) under the form of agglomerated crystals of meta-torbernite (a few millimeters in length for larger ones) and black host rock. The sample was crushed manually using an agate mortar to obtain a powder as fine as the synthesized product. It was purified through two cycles of washing by centrifugation (4 min at 4500 rpm) in a solution of HNO_3 (1 mol L^{-1}), then in deionized water. After these cycles, the black host rock was separated from the meta-torbernite by sedimentation. The resulting solid corresponded to mainly natural meta-torbernite with trace amounts of black host rock. It was then characterized by the same techniques than synthetic meta-torbernite.

2.2. Characterizations

Powder X-ray Diffraction (PXRD) patterns were recorded by the use of the Bruker D8 diffractometer equipped with the LynxEye detector adopting the Bragg–Brentano geometry and using Cu $K\alpha_{1,2}$ radiation ($\lambda = 1.5418$ Å). Data were recorded at room temperature in the $5^{\circ} < 2\theta < 100^{\circ}$ range with a step size $\Delta(2\theta) = 0.02^{\circ}$ and a total counting time of about 1.5 h. The unit cell parameters were refined by the Rietveld method using the Thomson-Cox-Hastings Pseudo Voigt function convoluted with an axial divergence asymmetry function available in the Fullprof_Suite program [20]. Pure silicon was used as standard in order to extract the instrumental functions.

SEM observations were conducted using a FEI Quanta 200 electron microscope, equipped either with a large field detector (LFD) or a backscattered electron detector (BSED), in high vacuum conditions with a very low accelerating voltage (2–3.1 kV). These conditions were chosen in order to create a beam deceleration effect that led to high resolution images. Powdered samples were then directly analyzed without any additional preparation step such as metallization.

To check the stoichiometry of the prepared meta-torbernite samples, X-EDS analyses were performed with the SEM device, using a Bruker XFlash 5010 detector. In order to determine quantitatively the elemental atomic percentages as well as the mole ratios, the powders were first embedded in an epoxy resin. The surface of the sample was then polished to reach an optical grade and metallized by carbon deposition. Experimental data were finally collected from 30 different points using UO_2, apatite $Ca_5(PO_4)_3F$ and Cu metal as internal references. In addition, elemental concentrations were determined by ICP-AES (Spectro Arcos EOP) after complete dissolution of an aliquot of the solid in a 4 mol L^{-1} HNO_3 solution. This apparatus was also used to follow the evolution of the uranium, copper, and phosphorus concentrations during precipitation and dissolution experiments. Calibration was performed with SPEX standard solutions ($0.5 < C_U < 30$ mg L^{-1}, $0.075 < C_P$ or $C_{Cu} < 4.5$ mg L^{-1}).

Raman spectra were recorded with a Horiba-Jobin Yvon Aramis apparatus using a Nd:YAG laser (532 nm) delivering 60 mW power at the sample surface and associated edge filter. The laser beam was focused on the sample by an Olympus BX 41 microscope, with a spot size of about 1 μm^2. For each spectrum, a dwell time of 10 s was used with an average of three scans.

Thermogravimetric analyses (TGA) and differential thermal analyses (DTA) were performed in air on a Setsys Evolution apparatus provided by Setaram with a heating rate of 5 K min^{-1} up to 1273 K.

Finally, the specific surface area (S_{BET}) of the synthesized meta-torbernite samples was determined by krypton adsorption/desorption at 77 K using a MJ Micromeritics ASAP 2020 apparatus (BET method). The samples were outgassed at 333 K for three days before the analysis.

2.3. Supersaturation and undersaturation solubility experiments

Thermodynamic equilibrium was approached either by supersaturation (during the precipitation experiment) or by undersaturation (during the dissolution experiments). In the case of equilibrium, both methods lead to the same saturation index.

The precipitation of meta-torbernite was monitored through regular uptakes of the leachate (50 or 100 μL). Aliquots were first centrifuged (2 min at 14,000 rpm) to eliminate potential colloids and nanometric particles with average size less than 65 nm, for further elemental concentration measurements by ICP-AES [21]. The sampled volumes were replaced by fresh solution to maintain a constant volume throughout the experiment. In these conditions, less than 3% of the leachate was renewed in order to avoid any perturbation in the establishment of saturation processes at the solid/liquid interface. The pH of the solution was checked several times during the experiment, once the steady state was reached. The pH of solution was finally measured by determining the concentration of protons from a standard curve obtained by measuring the pH of titrated nitric acid solutions (C_H^+ between 5×10^{-3} and 2.5×10^{-7} mol L^{-1}) in which the ionic strength was set to 1 mol L^{-1} by adding a KNO_3, KCl or K_2SO_4 solution according the anion present in the supernatant studied. The system was considered to be at equilibrium when the results of at least three consecutive analyses, by considering an interval equal to at least twice the time required to initially reach the steady state (few hours for supersaturation experiments and few days for oversaturation ones), were in the range of two standard deviations of the analyses. The average composition of the solution at saturation with respect to the solid phase was calculated as the average of consecutive analyses that did not significantly differ from one another. Once equilibrium was reached, the remaining solid was separated from the supernatant by centrifugation (6 min at 4500 rpm) and analyzed by PXRD, SEM, X-EDS and ICP-AES (after total dissolution in 4 mol L^{-1} HNO_3 to determine the sample stoichiometry) without any preliminary washing step to prevent degradation of potential neoformed phases.

Prior the leaching test, the powdered samples were washed with deionized water, then with the medium used for dissolution. 800 mg of meta-torbernite were then introduced into sealed polytetrafluoroethylene (PTFE) containers (from Savillex) with 5 mL of acid solution (1 mol L^{-1} HNO_3, 1 mol L^{-1} HCl, or 1 mol L^{-1} H_2SO_4). The containers were potentially placed into an oven to study the effect of temperature (277 K, 313 K, and 353 K). The dissolution of the solid was monitored following the same protocol as for the precipitation experiments.

2.4. Thermodynamic interpretation

The solubility constant was calculated from super- and under saturation experiments once a steady state was reached and only when the reaction was found to be congruent, that is to say that no secondary phase precipitated and that the mole ratios of the constituent elements (U, P and Cu) in the solution corresponded to the stoichiometry of the meta-torbernite sample. Considering the predominant species under the conditions used (very low pH), the dissolution of meta-torbernite could thus be written as follows:

$$(H_3O)_{0.4}Cu_{0.8}(UO_2)_2(PO_4)_2 \cdot 7.6H_2O + 5.6H_3O^+ \leftrightarrows 0.8Cu^{2+} + 2UO_2^{2+} + 2H_3PO_4 + 13.6H_2O \tag{1}$$

Following Eq. (1), the solubility constant ${}^*K_s^\circ$ was calculated using the relation with species activities:

$${}^*K_s^\circ = (H_3O^+)^{-5.6} \times (Cu^{2+})^{0.8} \times (UO_2^{2+})^2 \times (H_3PO_4)^2 \tag{2}$$

where (i) denotes activity of ion i and the asterisk corresponds to a solubility constant which simultaneously involves protonation equilibrium [12].

The activities of species were calculated from elemental concentrations using PHREEQC-2 software [22] with the Minteq.v4 database [23] that takes into account the main reactions involving the considered species (all the thermodynamic data used for these calculations are listed in Table S1: Supporting Information). PHREEQC-2 allowed determining activity corrections using specific interaction theory (SIT) [12]:

$$\log(\gamma_i) = -\frac{z_i^2 A\sqrt{I_m}}{1 + 1.5 \times \sqrt{I_m}} + \sum_j \varepsilon_{(i,j,I)} m_j \tag{3}$$

where m_j is the molality of species j (mol kg^{-1}); $\varepsilon_{(i,j)}$ is the SIT coefficient between ion i and counter-ion j. In addition, the A parameter variation versus temperature was taken from the literature and $\varepsilon_{(i,j)}$ was considered to be independent of temperature [12].

Table 1
Ion interaction coefficient $\varepsilon_{(i,j)}$ values used in this work.

	NO_3^-	Cl^-	HSO_4^-	SO_4^{2-}
Cu^{2+}	0.11 ± 0.01 [12]	0.08 ± 0.01 [12]	0.32 ± 0.05[a]	–
H^+	0.07 ± 0.01 [12]	0.12 ± 0.01 [12]	0.17 ± 0.06[a]	−0.03 ± 0.05[a]
UO_2^{2+}	0.24 ± 0.03 [12]	0.21 ± 0.02 [12]	0.46 ± 0.05[a]	0.12 ± 0.05 [24]

[a] Values estimated by analogy with ions of the same charge and similar size (Li^+ for H^+ and ClO_4^- for HSO_4^-) [25-27].

The concentrations of the ions coming from the dissolution media were several orders of magnitude higher than those of the reacting species. Hence, they induced the main contribution to the $\log(\gamma_i)$ value. This led us to simplify the summation $\sum_j \varepsilon_{(i,j,I)} m_j$, so that only ion interaction coefficients between the ionic species of interest and that associated with the dissolution medium were taken into account. The values of $\varepsilon_{(i,j)}$ used in the calculations are indicated in Table 1.

According to the NEA [12], the conventional solubility constants are calculated using uncomplexed aqueous species. For meta-torbernite, the dissolution equilibrium studied is the followed:

$$(H_3O)_{0.4}Cu_{0.8}(UO_2)_2(PO_4)_2 \cdot 7.6H_2O \leftrightarrows 0.4H_3O^+ + 0.8Cu^{2+} + 2UO_2^{2+} + 2PO_4^{3-} + 7.6H_2O \tag{4}$$

This equilibrium was also considered to calculate the solubility constant in supersaturated experiments.

The conventional standard solubility constant of this equilibrium was thus:

$$K^\circ_{s,0} = (H_3O^+)^{0.4} \times (Cu^{2+})^{0.8} \times (UO_2^{2+})^2 \times (PO_4^{3-})^2 \tag{5}$$

where “0” indicates that dissolution equilibrium involving only uncomplexed aqueous species [12].

The calculated value for (PO_4^{3-}) is close to 10^{-23} mol L^{-1}, but determined with a high uncertainty due to numerical computation. In order to minimize the error in calculating the solubility constant, the solubility constant of equilibrium (5) was then deduced from $^*K^\circ_s$ and from the acidity constants of H_3PO_4 using the following equation:

$$K^\circ_{s,0} = {}^*K^\circ_s \times (K_{a1}K_{a2}K_{a3})^2 \tag{6}$$

where K_{a1}, K_{a2} and K_{a3} are the phosphorus acid constants related to $H_3PO_4/H_2PO_4^-$ ($pK_{a1} = 2.14$), $H_2PO_4^-/HPO_4^{2-}$ ($pK_{a2} = 7.21$), and HPO_4^{2-}/PO_4^{3-} ($pK_{a3} = 12.35$) [12], respectively.

The associated standard Gibbs free energy was calculated from conventional standard solubility constant $K^\circ_{s,0}$ using the following equation:

$$\Delta_R G^\circ(T) = -R \times T \times \ln(K^\circ_{s,0}(T)) \tag{7}$$

where R is the gas constant and T absolute temperature (K).

When $\Delta_R H^\circ$ and $\Delta_R S^\circ$ dependency with temperature can be neglected in the studied temperature range (which is commonly admitted for small temperature ranges), the standard Gibbs free energy of the dissolution reaction was calculated from the standard enthalpy and standard entropy of reaction according to:

$$\Delta_R G^\circ(T) = \Delta_R H^\circ - T\Delta_R S^\circ \tag{8}$$

Combining Eqs. (8) and (9) leads to:

$$\ln K^\circ_s(T) = \frac{-\Delta_R H^\circ}{RT} + \frac{\Delta_R S^\circ}{R} \tag{9}$$

Based on the calculated values of $\Delta_R G^\circ(298\text{ K})$, $\Delta_R H^\circ(298\text{ K})$ and $\Delta_R S^\circ(298\text{ K})$ associated with reaction (1) and according to the Hess’s law, the standard Gibbs free energy and enthalpy associated with the formation of meta-torbernite from its constituent elements, $\Delta_f G^\circ$, $\Delta_f H^\circ$ and $\Delta_f S^\circ$ were determined using Eqs. ((10) and (11)):

$$\begin{aligned}\Delta_f X^\circ(\text{meta-torbernite}) = {} & 0.8 \times \Delta_f X^\circ(Cu^{2+}) + 0.4 \times \Delta_f X^\circ(H^+) \\ & + 2 \times \Delta_f X^\circ(UO_2^{2+}) + 2 \\ & \times \Delta_f X^\circ(PO_4^{3-}) + 8 \times \Delta_f X^\circ(H_2O) \\ & - \Delta_R X^\circ(\text{Eq.1})\end{aligned} \tag{10}$$

where $X = G$ or H;

$$\begin{aligned}\Delta_f S^\circ(\text{meta-torbernite}) = {} & S^\circ_m(\text{meta-torbernite}) - 0.8 \\ & \times S^\circ_m(9m(\text{cr})) - 0.4 \times S^\circ_m(H^+) - 8 \\ & \times S^\circ_m(H_2(\text{g})) - 2 \times S^\circ_m(U(\text{cr})) - 2 \\ & \times S^\circ_m(P(\text{cr})) - 10 \times S^\circ_m(O_2(\text{g}))\end{aligned} \tag{11}$$

i.e.:

$$\begin{aligned}S^\circ_m(\text{meta} - \text{torbernite}) = {} & 0.8 \times S^\circ_m(Cu^{2+}) + 0.4 \times S^\circ_m(H^+) + 2 \\ & \times S^\circ_m(UO_2^{2+}) + 2 \times S^\circ_m(PO_4^{3-}) + 8 \\ & \times S^\circ_m(H_2O) - \Delta_R S^\circ(\text{Eq.1})\end{aligned} \tag{12}$$

The thermodynamic data [12] of the species used to determine the enthalpy, Gibbs free energy and entropy associated with the formation of meta-torbernite are supplied in the supporting information (Table S2).

3. Results and discussion

3.1. Characterization of synthesized meta-torbernite and comparison with natural samples

The recorded PXRD patterns are viewed in Fig. 1. Purified natural and synthesized samples exhibit similar patterns containing mainly the meta-torbernite (JCPDS file #01-072-7383 [28]). However, the PXRD pattern of the natural sample showed additional lines, corresponding to remaining impurities in the sample, despite the multiple washing steps. The PXRD pattern of the natural sample before purification showed the presence silica SiO_2 (cristobalite) and aluminum phosphate $AlPO_4$, which are commonly found in uraniferous sites. Moreover, the presence of calcite ($CaCO_3$,00-004-0637) was detected with a main intense reflection around $2\theta = 30°$. This peak corresponds to the sample holder (Plasticine) used for the natural sample.

The refinement of the PXRD pattern of synthetic meta-torbernite (SG: P4/n) led to $a = 6.985(1)$ Å, $c = 17.3294(2)$ Å, and $V = 841.53(2)$ Å, which appeared consistent with values reported by Locock and Burns [28]. The presence of other phases in the natural sample made difficult the refinement of the PXRD pattern. However, there was no significant differences between the XRD peaks of the two samples and therefore the impurities present in the natural sample did not significantly affect its structure.

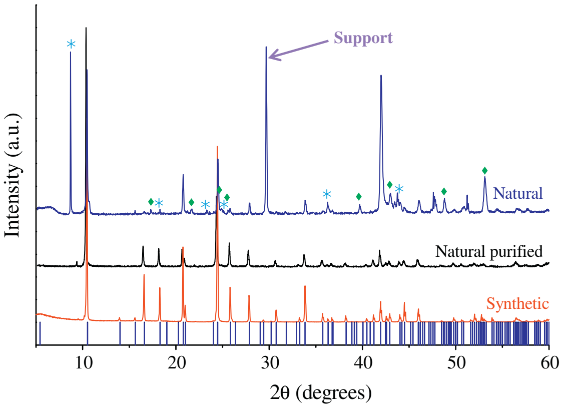

Fig. 1. PXRD patterns of synthesized (red), purified natural (black) – used for dissolution experiments – and raw natural (blue) meta-torbernite samples. The XRD lines associated with cristobalite (SiO_2) and $AlPO_4$ are indicated by ● (JCPDS file #01-085-0621 [29]) and ▲ (JCPDS file #00-045-0177 [30]), respectively. (For interpretation of the references to color in this figure legend, the reader is referred to the web version of this article.)

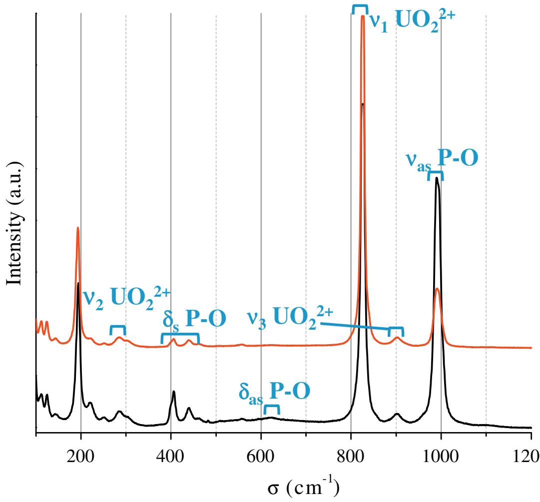

Fig. 2. Raman spectra of purified natural (red) and synthetic (black) samples of meta-torbernite. (For interpretation of the references to color in this figure legend, the reader is referred to the web version of this article.)

Table 2
X-EDS analyses (expressed in atomic percentage) of purified natural and synthetic samples of meta-torbernite.

	Purified natural sample	Synthetic sample	Calculated[a]
U (at.%)	12.4 ± 0.3	12.2 ± 0.4	11.8
P (at.%)	11.4 ± 0.5	13 ± 1	11.8
Cu (at.%)	5 ± 1	4.1 ± 0.9	5.9

[a] Assuming the chemical formula $Cu(UO_2)_2(PO_4)_2{\cdot}8H_2O$.

Both samples were also characterized by Raman spectroscopy. All the characteristic bands associated with phosphate and uranyl entities were observed in the collected spectra with close wave numbers for synthetic and natural samples (Fig. 2 and Table S3). For example, the symmetric (ν_1) and antisymmetric (ν_3) stretching mode of the UO_2^{2+} unit occured respectively at 822 and 895 cm^{-1} for the synthetic sample and at 824 and 893 cm^{-1} for the natural one. It was the same for the antisymmetric stretching mode of the PO_4^{3-} unit which occured at 989 cm^{-1} for the synthetic compound and at 987 cm^{-1} for the natural one. These observations mean that the bond lengths in the uranyl and phosphate groups, and therefore their environment, were similar for both compounds and confirm that the two samples had the same structure, despite impurities present in the natural sample.

In the structure, uranyl and phosphate groups form parallel layers. Copper and water molecules are intercalated between layers. The consequence of this 2D arrangement is the formation of platelet-shaped grains as observed by SEM for both synthesized and natural samples (Fig. 3). However, despite their similar morphology and grain size (a few hundred micrometers), the specific surface area differed for the samples: 0.4 ± 0.2 $m^2\ g^{-1}$ for synthetic samples, versus 2.6 ± 0.2 $m^2\ g^{-1}$ for natural samples. This difference was probably due to the different granulometry of the samples. Natural meta-torbernite sample exhibited heterogeneous particle size distribution compared to the synthetic one. In addition, the natural sample could have been altered (by meteoric or underground water, or during the purification protocol) leading to an increase of the surface roughness.

The stoichiometry of both samples was determined by X-EDS analyses (Table 2) coupled with SEM. It suggested that both samples were copper-depleted compared to the expected

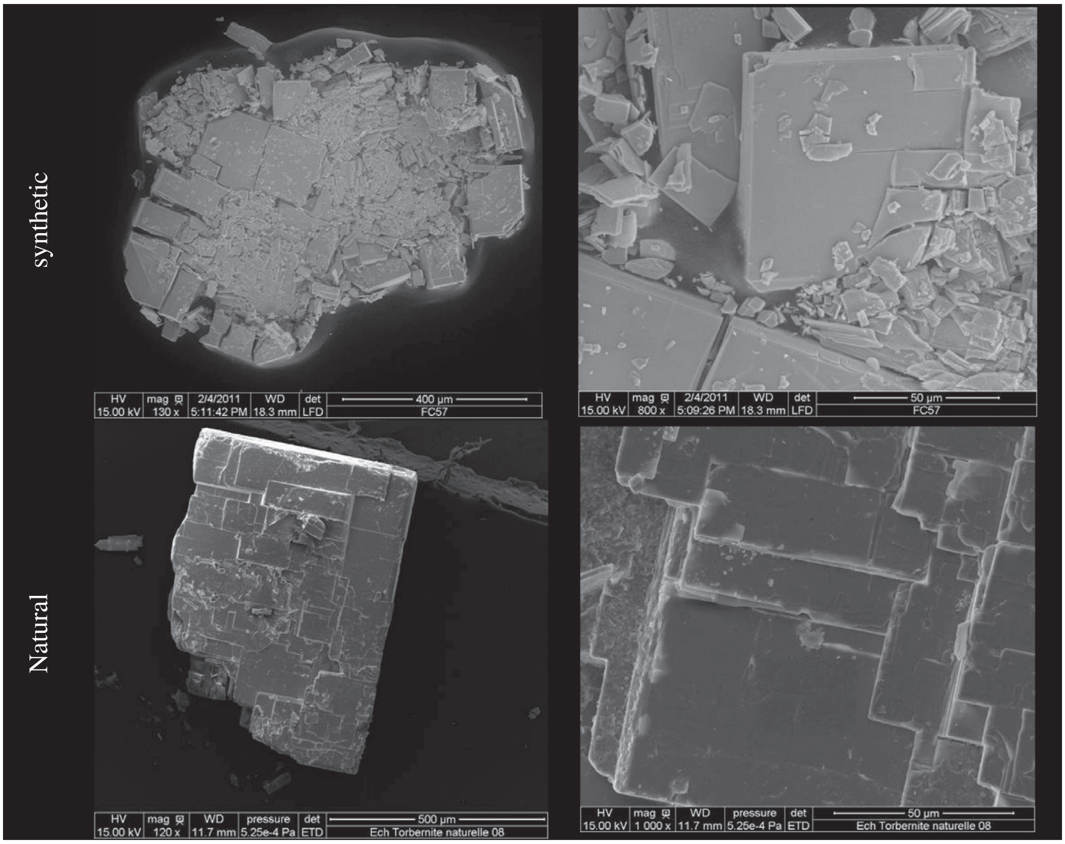

Fig. 3. SEM micrographs of synthetic and natural meta-torbernite samples.

stoichiometry. This lack of copper was also confirmed by ICP-AES analyses after the complete dissolution of the solid. The deficit in the charge balance was thus assumed to be ensured by H^+ ions, which are surely linked to water molecules present in the interlayer spaces. In addition, the hydration rate (~8 H_2O) was determined by TGA–DTA experiments. The resulting chemical formula for both samples was $(H_3O)_{0.4}Cu_{0.8}(UO_2)_2(PO_4)_2{\cdot}7.6H_2O$ ($8H_2O$ of hydration rate = $7.6H_2O + 0.4H_3O^+$). In addition, the other detected elements at a trace level by X-EDS and ICP-AES were Mn, Co and Fe. They were probably incorporated by direct substitution for copper in the meta-torbernite structure, without affecting the structure of the compound.

Based on all the characterization techniques, both synthetic and natural meta-torbernite samples presented the same stoichiometry and similar morphology. However, the natural sample was found to be polyphasic since it still contains cristobalite (SiO_2) and aluminum phosphate ($AlPO_4$) from the host rock. These elements were analyzed during the dissolution tests by ICP–OES then were taken into account during the speciation calculation. Because of the presence of these impurities in the natural sample, the study of synthetic sample became essential and was studied firstly.

3.2. Solubility data related to synthetic meta-torbernite

3.2.1. Supersaturation experiments

The precipitation of synthetic meta-torbernite corresponds to the supersaturation experiments, through the monitoring of changes in the reactant concentrations. The elemental concentrations obtained at 303 K and 333 K are plotted versus the precipitation time in Fig. 4; the other experiments are presented in Fig. S1. For most of the experiments, stoichiometric precipitation was clearly observed. The P:U and Cu:U mole ratio determined in solution corresponded to the stoichiometry of meta-torbernite (U:P:Cu = 1:1:0.4) throughout the experiment even if the slight excess of phosphoric acid and/or copper chloride introduced in the starting mixture led to slightly different mole ratios in solution at equilibrium.

In order to evaluate the precipitation rate associated with reaction (1), a first-order kinetic law was assumed:

$$-\frac{1}{n_i} \times \frac{dC_i}{dt} = k_i \times (C_i - C_{eq,i}) \tag{13}$$

where n_i is the stoichiometric coefficient of element i in the solid; C_i is the concentration of element i, $C_{eq,i}$ the concentration at equilibrium (mol L^{-1}); and k_i is the kinetic constant (d^{-1}).

Integrating Eq. (14) gives Eq. (15):

$$C_i(t) = (C_{0,i} - C_{eq,i}) \times \exp(-n_i \times k_i \times t) + C_{eq,i} \tag{14}$$

where $C_{0,i}$ is the initial concentration of element i (mol L^{-1}).

The fit of the experimental data allowed the determination of the k_i constant (the value obtained for phosphorus at 333 K is presented in Fig. 4). which was evaluated for each element and temperature (Table 3). For a given temperature, k_i were identical for the three elements confirming that precipitation was congruent. Kinetic constants increased slightly with temperature, as already reported by Wellman et al. [31] for meta-autunite. From these data, the activation energy, E_A was evaluated as 35 ± 3 kJ mol^{-1}. This is consistent with the value obtained for similar systems like thorium–uranium phosphate–diphosphate [32] or other phosphate confinement matrices used for radioactive waste management [33], and corresponds to a surface controlled dissolution mechanism [34,32,35].

As the precipitation was stoichiometric with regard to meta-torbernite, the solubility constant was calculated from the elemental concentrations, C_{eq}, determined at equilibrium for each experiment. The C_{eq} values, calculated concentrations, activities of species involved in Eq. (1) and solubility constants ${}^*K^{\circ}_s(T)$ and $K^{\circ}_{s,0}(T)$ are indicated in Table 4. All the obtained values were consistent and close to that determined by Pekarek et al. [13] (K_s (298 K) = $(8 \pm 2) \times 10^{-53}$), who did not specify the model used to calculate the activities of the species involved in the dissolution reaction. At room temperature, the solubility constant determined from concentrations led to a higher value than that obtained from activities ($K_{s,0} = 1.0 \times 10^{-52}$ and $K^{\circ}_{s,0} = 1.1 \times 10^{-53}$, respectively). This difference was even more pronounced for undersaturated experiments involving solutions with higher ionic strengths. This comparison illustrated the importance of the activity correction model for extrapolating the experimental results obtained under specific conditions to standard conditions. The standard Gibbs free energy associated with reaction (5), $\Delta_R G^{\circ}$, was always between 300 and 333 kJ mol^{-1} (Table 4).

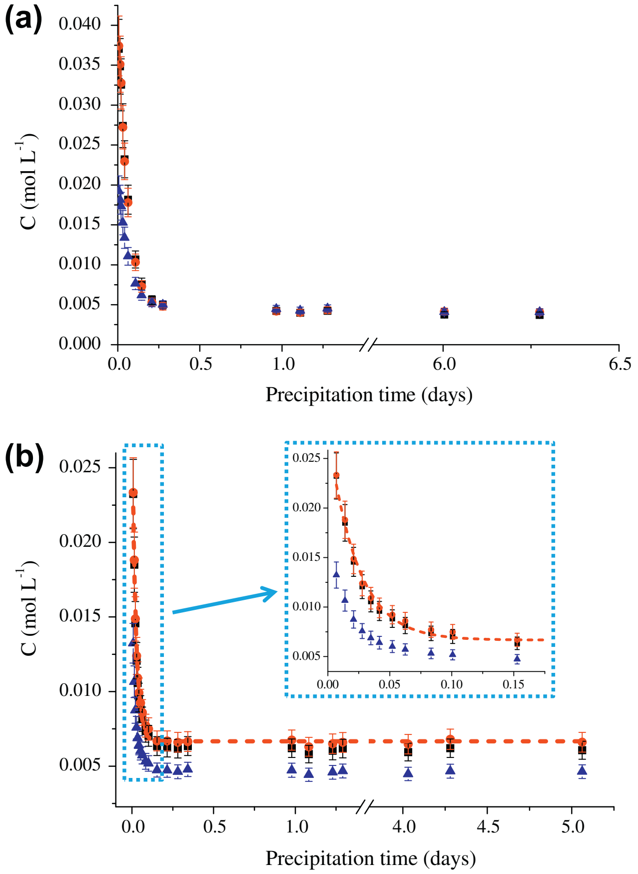

Fig. 4. Evolution of elemental concentrations C_U (■), C_P (●) and C_{Cu} (▲) determined by ICP-AES during the precipitation of meta-torbernite at 303 K (a) and 333 K (b) in 0.2 mol L^{-1} of H_3PO_4 and focus on the early days of precipitation with fitting using formula reported in Eq. (15) for P at 333 K.

Table 3
Kinetic constant for each element associated to the meta-torbernite precipitation (over saturated experiments).

	k_U (d^{-1})	k_P (d^{-1})	k_{Cu} (d^{-1})
296 K	7.1 ± 0.2	7.2 ± 0.2	6.66 ± 0.09
303 K	15 ± 1	15 ± 1	13.4 ± 0.7
309 K	25 ± 2	20 ± 4	23 ± 2
327 K	35 ± 4	38 ± 4	36 ± 2
333 K	41 ± 4	42 ± 4	34 ± 4

3.2.2. Undersaturation experiments

The evolution of the elemental concentration obtained during the dissolution of synthetic meta-torbernite in 1 mol L^{-1} HNO_3, 1 mol L^{-1} HCl, and 1 mol L^{-1} H_2SO_4 at 296 K are viewed in Fig. 5 (other results are included in supporting information: Fig. S2). As observed for oversaturation experiments, meta-torbernite dissolution was found to be congruent whatever the experimental conditions considered. A plateau was reached within 5 days at 296 K. The time required to reach this plateau decreased significantly as the temperature increased (from 6 days at 277 K to 2 days at 313 K) whatever the dissolution medium considered. Unlike oversaturated experiments, zero-order kinetics were therefore considered to estimate the dissolution rate which was calculated on the first 12 h of the dissolution. Table 5 includes the kinetic constants in each medium for each element. Kinetic constants determined in the three media were similar. On this basis, sulfate anions did not play any significant role in the dissolution mechanism, conversely to that was reported during the dissolution of ThO_2 [36] or of thorium uranium-doped britholite ceramics [37] and ascribed to the higher complexation constant of phosphates with uranyl compared to nitrates or chlorides. In our experiments, the phosphate entities present in meta-torbernite probably counterbalanced the complexing role of sulfate ions at the solid–liquid interface since they are the major complexing species for uranyl (log K $(UO_2(HPO_4)_2^{2-})$ = 42.99 and log K $(UO_2(SO_4)_2^{2-})$ = 4.14). Phosphate ions thus "protected" uranyl from complexation with sulfate ions, which was obviously not the case for oxides where this competition did not exist.

Whatever the media considered, the kinetic constants were slower than those associated with precipitation (e.g. $k_{diss,U} = 0.035 \pm 0.005$ mol L^{-1} d^{-1} and $k_{prec,U} = 0.234 \pm 0.009$ mol L^{-1} d^{-1} at 296 K). This was already suggested by Gorman-Lewis et al. [38] who reported reaching steady-state conditions within 1 day during supersaturated experiments and within 6 days for undersaturation experiments during the dissolution of natural meta-autunite. In addition, the activation energy related to the dissolution reaction reached 52 ± 4 kJ mol^{-1} and argued for the existence of a surface-controlled dissolution mechanism and is similar to that obtained for precipitation ($E_A = 35 \pm 3$ kJ mol^{-1}).

For each experiment, the elemental concentrations at equilibrium C_{eq}, the activities of the species involved in the reaction (1), the solubility constant values $^{*}K_s^{\circ}(T)$ and $K_{s,0}^{\circ}(T)$, as well as the standard Gibbs free energy associated with the meta-torbernite dissolution reaction (5) are indicated in Table 6.

The solubility products were found to be independent of the dissolution medium, confirming the validity of the activity correction model. It is important to note that supersaturated and undersaturated experiments performed at the same temperature led to similar solubility product values. As the reversibility of the equilibrium was evidenced, a thermodynamic equilibrium state was reached in both cases that allowed thermodynamic interpretation of the results. The values obtained for the solubility product of meta-torbernite were lower than previously published, except by Pekarek et al. [13] who found a value in the same range, K_s(298 K) = (8 ± 2) × 10^{-53}, and Ilton et al. [15] who reported K_s(298 K) = (2.3 ± 0.5) × 10^{-53}. Other published values [7,14] were not subject to a rigorous calculation of speciation, which may explain the higher published values. The very low solubility of meta-torbernite combined with the ubiquity of phosphate in the environment can thus explain the rather high occurrence of meta-torbernite in uranium ore deposits or in uranium-contaminated sites.

3.2.3. Determination of thermodynamic data associated with meta-torbernite

The variation of ln($K_{s,0}^{\circ}$) versus the reciprocal temperature obtained from supersaturation and undersaturation experiments is plotted in Fig. 6. Using Eq. (10), a linear regression of these data allowed calculating the $\Delta_R H^{\circ}$ and $\Delta_R S^{\circ}$ values associated with reaction (1) (Table 7). The latter were not influenced by the medium ($\Delta_R H^{\circ}$ = 40 and 53 kJ mol^{-1} and $\Delta_R S^{\circ}$ = −879 and −820 J mol^{-1} K^{-1} respectively in 1 mol L^{-1} HCl and 1 mol L^{-1} H_2SO_4 for undersaturated experiments) and were similar in super- and undersaturated experiments ($\Delta_R H^{\circ}$ = 39 kJ mol^{-1} and $\Delta_R S^{\circ}$ = −878 J mol^{-1} K^{-1} for supersaturated experiments). The dissolution reaction was thus found to be endothermic. Nevertheless in the studied temperature range, the influence of temperature was found to be weak. Indeed, as shown in Fig. 6, the linear regression of the data obtained for both conditions (super- and undersaturation) led to a low value for $\Delta_R H^{\circ}$ indicating a rather low temperature dependence.

The calculated values of $\Delta_R G^{\circ}$, $\Delta_R H^{\circ}$ and $\Delta_R S^{\circ}$ associated with reaction (1) at 298 K were used in Hess's law (Eq. (10)) to determine the thermodynamic data associated with the formation of

Table 4
$^{*}K_s^{\circ}$(T), $K_{s,0}^{\circ}(T)$ and $\Delta_R G^{\circ}$ values associated with meta-torbernite dissolution from oversaturated experiments.

T (K)	Element	C_{eq} (× 10^{-3} mol L^{-1})	Species	C_{eq} (× 10^{-3} mol L^{-1})	Activity	$^{*}K_s^{\circ}(T)$ (× 10^{-10})	$K_{s,0}^{\circ}(T)$ (× 10^{-53})	$\Delta_R G^{\circ}(T)$ (kJ mol^{-1})
296	U	2.7 ± 0.1	UO_2^{2+}	1.99 ± 0.07	(5.5 ± 0.2) × 10^{-4}			
	P	6.2 ± 0.1	H_3PO_4	5.48 ± 0.09	(5.5 ± 0.1) × 10^{-3}	2 ± 0.5	1.1 ± 0.2	300.5 ± 0.4
	Cu	2.9 ± 0.1	Cu^{2+}	2.39 ± 0.08	(6.7 ± 0.2) × 10^{-4}			
	pH = 0.76 ± 0.05		H^+	232 ± 6	(2.0 ± 0.5) × 10^{-1}			
303	U	4.0 ± 0.4	UO_2^{2+}	3.2 ± 0.3	(9.4 ± 0.9) × 10^{-4}			
	P	4.0 ± 0.4	H_3PO_4	3.5 ± 0.3	(3.5 ± 0.4) × 10^{-3}	4 ± 2	1.5 ± 0.9	307 ± 2
	Cu	4.0 ± 0.4	Cu^{2+}	3.3 ± 0.3	(9.0 ± 0.9) × 10^{-4}			
	pH = 0.75 ± 0.05		H^+	200 ± 20	(2.1 ± 0.2) × 10^{-1}			
309	U	3.1 ± 0.3	UO_2^{2+}	2.3 ± 0.2	(6.3 ± 0.6) × 10^{-4}			
	P	8.1 ± 0.8	H_3PO_4	7.3 ± 0.7	(7.3 ± 0.7) × 10^{-3}	4 ± 2	1.7 ± 0.9	312 ± 2
	Cu	3.9 ± 0.4	Cu^{2+}	3.2 ± 0.3	(8.2 ± 0.9) × 10^{-4}			
	pH = 0.70 ± 0.05		H^+	270 ± 10	(2.0 ± 0.1) × 10^{-1}			
327	U	4.8 ± 0.5	UO_2^{2+}	3.7 ± 0.4	(1.0 ± 0.1) × 10^{-3}			
	P	9.7 ± 0.9	H_3PO_4	8.7 ± 0.8	(8.7 ± 0.8) × 10^{-3}	13 ± 7	5 ± 3	328 ± 2
	Cu	6.4 ± 0.6	Cu^{2+}	5.3 ± 0.5	(1.3 ± 0.1) × 10^{-3}			
	pH = 0.67 ± 0.05		H^+	210 ± 20	(2.2 ± 0.1) × 10^{-1}			
333	U	6.1 ± 0.6	UO_2^{2+}	5.0 ± 0.5	(1.3 ± 0.1) × 10^{-3}			
	P	6.6 ± 0.7	H_3PO_4	5.9 ± 0.6	(5.9 ± 0.6) × 10^{-3}	15 ± 8	6 ± 3	333 ± 2
	Cu	4.6 ± 0.5	Cu^{2+}	3.8 ± 0.4	(9 ± 1) × 10^{-4}			
	pH = 0.72 ± 0.05		H^+	260 ± 10	(1.9 ± 0.1) × 10^{-1}			

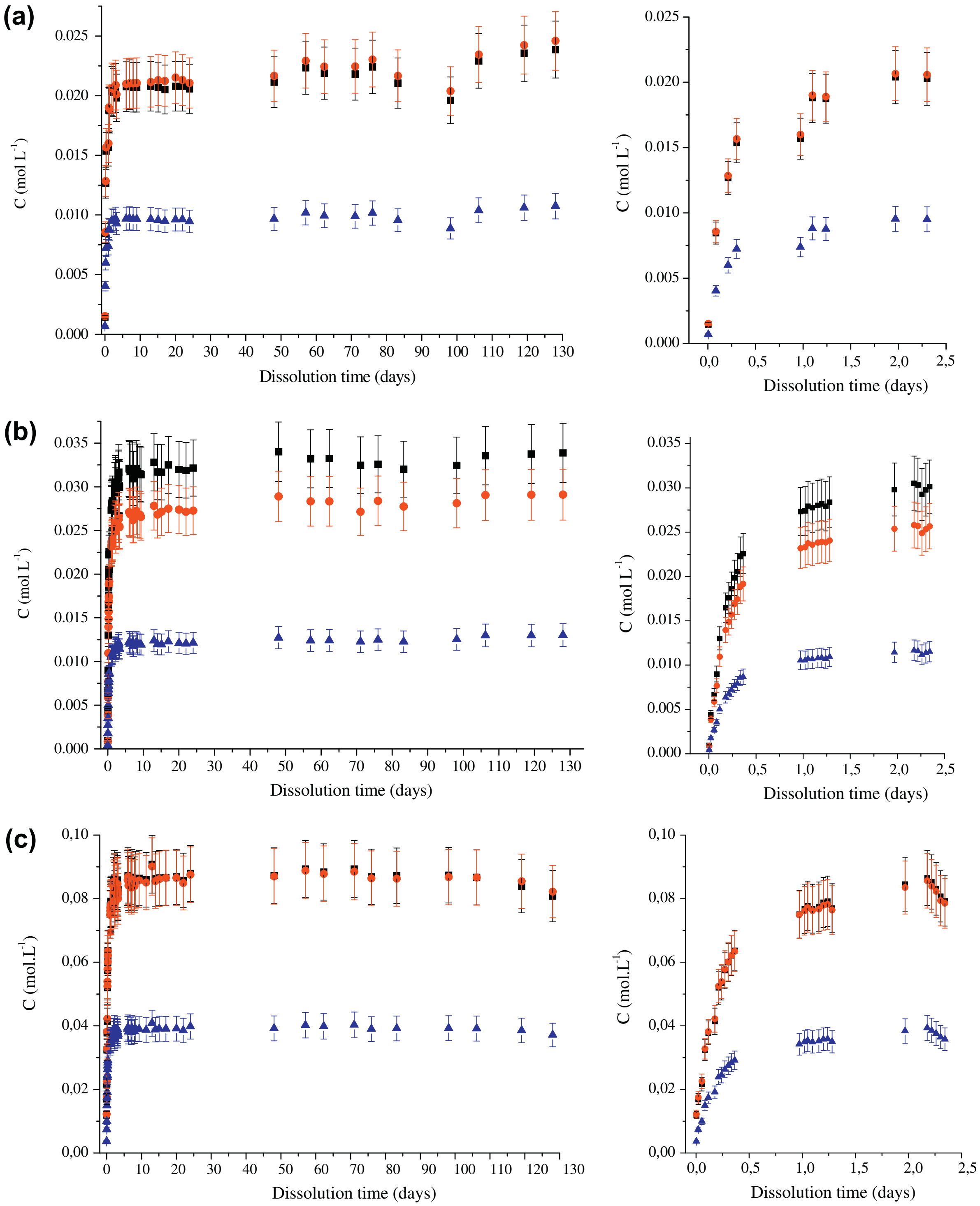

Fig. 5. Evolution of elemental concentrations C_U (■), C_P (●) and C_{Cu} (▲) measured by ICP-AES during the dissolution of synthetic meta-torbernite in 1 mol L^{-1} HNO_3, (a) 1 mol L^{-1} HCl, (b) and 1 mol L^{-1} H_2SO_4 and (c) at 296 K (left) and focus on the early days of dissolution (right).

meta-torbernite. The linear regression was not performed for nitric acid where the point at 277 K was not considered to be reliable (value lower than that obtained for the other two acids). Considering the uncertainty on thermodynamic data associated with the formation of meta-torbernite, the values obtained were in very good agreement: $\Delta_R G° = 300 \pm 2$ kJ mol^{-1} for all experiments, $\Delta_R H° = 40 \pm 3$, and 53 ± 9 kJ mol^{-1} and $\Delta_R S° = -879 \pm 7$, -820 ± 30 J mol^{-1} K^{-1} for experiments in HCl and H_2SO_4, respectively. The $\Delta_f G°$, $\Delta_f H°$ and $\Delta_f S°$ values obtained from the experiments in undersaturation and the average for oversaturation conditions are listed in Table 7, considering values obtained in HCl as input data. The formation reaction of meta-torbernite was thus favorable ($\Delta_f G° = -6100 \pm 5$ kJ mol^{-1}) and exothermic ($\Delta_f H° = -6890 \pm 10$ kJ mol^{-1}). In addition, Karyakin et al. [14] published values for the Gibbs free energy and the enthalpy of formation of meta-torbernite calculated from calorimetric measurements in the range 80–300 K

Table 5
Kinetic constants associated with the dissolution of meta-torbernite calculated from the concentration evolution of each element during undersaturation experiments.

		k_U mol L^{-1} d^{-1}	k_P mol L^{-1} d^{-1}	k_{Cu} mol L^{-1} d^{-1}
277 K	HNO_3	0.015 ± 0.003	0.016 ± 0.006	0.012 ± 0.002
	HCl	0.004 ± 0.002	0.009 ± 0.002	0.010 ± 0.002
	H_2SO_4	0.011 ± 0.004	0.010 ± 0.004	0.011 ± 0.002
296 K	HNO_3	0.03 ± 0.01	0.03 ± 0.01	0.029 ± 0.007
	HCl	0.035 ± 0.005	0.030 ± 0.002	0.028 ± 0.001
	H_2SO_4	0.039 ± 0.005	0.031 ± 0.005	0.031 ± 0.002
313 K	HNO_3	0.24 ± 0.03	0.18 ± 0.08	0.15 ± 0.02
	HCl	0.17 ± 0.06	0.21 ± 0.07	0.15 ± 0.02
	H_2SO_4	0.11 ± 0.07	0.12 ± 0.08	0.05 ± 0.04

Table 6
$^{*}K_s^{\circ}(T)$, $K_{s,0}^{\circ}(T)$ and $\Delta_R G^{\circ}$ values associated with the dissolution of meta-torbernite from undersaturated experiments.

T (K)	Medium	Element	C_{eq} ($\times 10^{-2}$ mol L^{-1})	Species	C_{eq} ($\times 10^{-2}$ mol L^{-1})	Activity	$^{*}K_s^{\circ}(T)$ ($\times 10^{-10}$)	$K_{s,0}^{\circ}(T)$ ($\times 10^{-53}$)	$\Delta_R G^{\circ}(T)$ (kJ mol^{-1})
277	1 mol L^{-1} HNO_3	U	2.04 ± 0.07	UO_2^{2+}	1.00 ± 0.03	$(2.71 \pm 0.09) \times 10^{-3}$			
		P	2.03 ± 0.07	H_3PO_4	1.81 ± 0.06	$(1.84 \pm 0.06) \times 10^{-2}$	0.25 ± 0.05	0.10 ± 0.02	286.6 ± 0.5
		Cu	0.78 ± 0.03	Cu^{2+}	0.43 ± 0.03	$(8.5 \pm 0.3) \times 10^{-4}$			
		pH = 0.16 ± 0.05		H^+	90 ± 10	0.7 ± 0.1			
	1 mol L^{-1} HCl	U	2.27 ± 0.05	UO_2^{2+}	1.58 ± 0.03	$(4.12 \pm 0.09) \times 10^{-3}$			
		P	2.21 ± 0.05	H_3PO_4	1.95 ± 0.04	$(1.95 \pm 0.04) \times 10^{-2}$	0.8 ± 0.1	0.31 ± 0.04	284 ± 0.3
		Cu	0.93 ± 0.02	Cu^{2+}	0.74 ± 0.02	$(1.45 \pm 0.03) \times 10^{-3}$			
		pH = 0.16 ± 0.05		H^+	90 ± 10	0.7 ± 0.1			
	1 mol L^{-1} H_2SO_4	U	7.1 ± 0.7	UO_2^{2+}	0.60 ± 0.06	$(2.55 \pm 0.03) \times 10^{-3}$			
		P	6.8 ± 0.7	H_3PO_4	6.8 ± 0.7	$(7.21 \pm 0.07) \times 10^{-2}$	2 ± 1	0.8 ± 0.4	282 ± 1
		Cu	3.2 ± 0.3	Cu^{2+}	2.0 ± 0.2	$(6.7 \pm 0.6) \times 10^{-3}$			
		pH = 0.10 ± 0.05		H^+	100 ± 10	0.9 ± 0.1			
296	1 mol L^{-1} HNO_3	U	2.42 ± 0.07	UO_2^{2+}	1.36 ± 0.04	$(3.6 \pm 0.1) \times 10^{-3}$			
		P	2.48 ± 0.06	H_3PO_4	2.25 ± 0.05	$(2.25 \pm 0.05) \times 10^{-2}$	2.3 ± 0.3	1.0 ± 0.1	300.8 ± 0.3
		Cu	1.08 ± 0.03	Cu^{2+}	0.64 ± 0.02	$(1.28 \pm 0.04) \times 10^{-3}$			
		pH = 0.20 ± 0.05		H^+	90 ± 10	0.6 ± 0.1			
	1 mol L^{-1} HCl	U	3.1 ± 0.3	UO_2^{2+}	1.9 ± 0.2	$(4.8 \pm 0.5) \times 10^{-3}$			
		P	3.1 ± 0.3	H_3PO_4	2.8 ± 0.3	$(2.8 \pm 0.3) \times 10^{-2}$	3 ± 1	1.1 ± 0.5	300 ± 1
		Cu	1.4 ± 0.1	Cu^{2+}	1.01 ± 0.07	$(1.9 \pm 0.1) \times 10^{-3}$			
		pH = 0.12 ± 0.05		H^+	100 ± 10	0.8 ± 0.1			
	1 mol L^{-1} H_2SO_4	U	8.3 ± 0.8	UO_2^{2+}	0.65 ± 0.06	$(2.8 \pm 0.3) \times 10^{-3}$			
		P	8.3 ± 0.8	H_3PO_4	8.3 ± 0.8	$(8.4 \pm 0.8) \times 10^{-2}$	5 ± 2	1.9 ± 0.9	299 ± 1
		Cu	3.8 ± 0.4	Cu^{2+}	2.6 ± 0.3	$(7.1 \pm 0.7) \times 10^{-3}$			
		pH = 0.10 ± 0.05		H^+	110 ± 10	0.9 ± 0.1			
313	1 mol L^{-1} HNO_3	U	4.2 ± 0.1	UO_2^{2+}	2.48 ± 0.06	$(6.2 \pm 0.1) \times 10^{-3}$			
		P	4.1 ± 0.1	H_3PO_4	3.56 ± 0.09	$(3.58 \pm 0.09) \times 10^{-2}$	16 ± 2	6.2 ± 0.7	313.1 ± 0.3
		Cu	1.77 ± 0.04	Cu^{2+}	1.06 ± 0.02	$(1.91 \pm 0.04) \times 10^{-3}$			
		pH = 0.18 ± 0.05		H^+	100 ± 10	0.7 ± 0.1			
	1 mol L^{-1} HCl	U	4.8 ± 0.5	UO_2^{2+}	2.5 ± 0.3	$(5.9 \pm 0.6) \times 10^{-3}$			315 ± 1
		P	4.7 ± 0.5	H_3PO_4	4.3 ± 0.5	$(4.3 \pm 0.5) \times 10^{-2}$	8 ± 2	3 ± 1	
		Cu	2.0 ± 0.2	Cu^{2+}	1.3 ± 0.1	$(2.1 \pm 0.2) \times 10^{-3}$			
		pH = 0.11 ± 0.05		H^+	90 ± 10	0.9 ± 0.1			
	1 mol L^{-1} H_2SO_4	U	9.9 ± 0.2	UO_2^{2+}	0.78 ± 0.02	$(3.02 \pm 0.06) \times 10^{-3}$			
		P	10.1 ± 0.2	H_3PO_4	10.1 ± 0.2	$(1.08 \pm 0.02) \times 10^{-1}$	25 ± 3	10 ± 1	311.8 ± 0.4
		Cu	4.2 ± 0.1	Cu^{2+}	3.22 ± 0.08	$(8.8 \pm 0.2) \times 10^{-3}$			
		pH = 0.07 ± 0.05		H^+	110 ± 10	0.1			

with an adiabatic vacuum calorimeter, which are very close to that determined in this work ($\Delta_f G^{\circ} = -6090 \pm 7$ kJ mol^{-1}, $\Delta_f H^{\circ} = -6885 \pm 8$ kJ mol^{-1} and $\Delta_f S^{\circ} = -2667 \pm 4$ J mol^{-1} K^{-1}), confirming that the method used in this work gives reliable values.

3.3. Solubility constant related to natural meta-torbernite

The variations of elemental concentrations obtained during dissolution experiments performed with a natural meta-torbernite sample in 1 mol L^{-1} HCl at 296 K are reported in Fig. 7a (data obtained in 1 mol L^{-1} HNO_3 and 1 mol L^{-1} H_2SO_4 are indicated in Fig. S3 and exhibit the same trends).

The dissolution of natural meta-torbernite was found to be incongruent. Indeed, while the uranium and phosphorus concentrations increased until a plateau was reached, the copper concentration decreased drastically after only one to two days of dissolution. However, a focus on the early days of dissolution (Fig. 7b) showed that the uranium, phosphorus and copper concentrations rose sharply and quickly during the first few minutes of the experiments, that is to say before the first point. The elemental release rates were thus calculated based on this single point, which implied a large uncertainty on these values.

Then the elemental concentrations of uranium, phosphorus and copper decreased until they reached a plateau. A steady state was

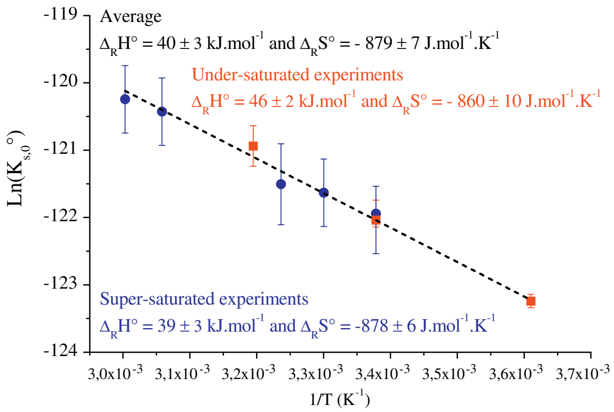

Fig. 6. Variation of Ln($K^{\circ}_{s,0}$) versus the reciprocal temperature during oversaturation (●) and undersaturation (🟥) experiments for synthetic meta-torbernite in 1 mol L^{-1} HCl.

then reached after 30 days of dissolution whatever the dissolution medium considered.

Fig. 8 highlights the comparison between synthetic and natural sample dissolution and showed that the same steady state was obviously reached for both types of samples. In the case of the natural sample, the higher release of uranium, copper and phosphorus in the early dissolution stage might be explained by the higher specific surface area of natural meta-torbernite (2.60 ± 0.30 m g^{-1} vs. 0.35 ± 0.2 m^2 g^{-1} for synthetic sample). Thus, from a kinetic point of view, the dissolution rate of the natural sample should be ten times higher, which was confirmed by the kinetic constants summarized in Table 8. Other factors could explain the rapid dissolution of the natural meta-torbernite. Impurities present in the natural sample could affect the dissolution rate. Additionally, irradiation damage could also modify the dissolution rate. Indeed, the natural sample, obviously older than the freshly synthesized sample, was subject to self-irradiation that could alter the specific surface area and the crystallization state [39,40]. This amorphization could increase the dissolution rate, as already reported for other phosphate materials such as thorium phosphate diphosphate [41] or monazite [42]. Finally, if the dissolution kinetics were influenced by the self-irradiation process, this was not the case for the thermodynamic data associated with the dissolution or the precipitation of meta-torbernite.

As the solid was dissolved very quickly at the beginning of the experiments, the solutions became supersaturated with regard to the solubility of meta-torbernite and led to the rapid precipitation of this phase until thermodynamic equilibrium was reached. Meta-torbernite thus still controlled the equilibrium and the solubility constant of meta-torbernite was also calculated. Indeed, the obtained values indicated in Table 8 ($K_{s,0}$°(298 K) = (2 ± 1) × 10^{-53}, $K^{\circ}_{s,0}$(298 K)= (2 ± 1) × 10^{-53} and $K^{\circ}_{s,0}$(298 K) = (4 ± 2) × 10^{-53} in 1 mol L^{-1} HNO_3, HCl, and H_2SO_4, respectively) were not significantly different from those obtained with the synthetic phase.

On this basis, the very good agreement on the solubility constant values obtained from direct precipitation or dissolution of both synthetic and natural meta-torbernite ($K^{\circ}_{s,0}$(298 K) =

Table 7
Thermodynamic data associated with the dissolution of synthetic meta-torbernite, calculated from supersaturation and undersaturation experiments and with the reaction of formation of meta-torbernite $\Delta_f G°$, $\Delta_f H°$ and $\Delta_f S°$ at 298 K.

	$\Delta_R G°$(298 K) (kJ mol^{-1})	$\Delta_R H°$(298 K) (kJ mol^{-1})	$\Delta_R S°$(298 K) (J mol^{-1} K^{-1})	$\Delta_f G°$(298 K) (kJ mol^{-1})	$\Delta_f H°$(298 K) (kJ mol^{-1})	$\Delta_f S°$(298 K) (J mol^{-1} K^{-1})
Oversaturation experiments						
	300 ± 1	39 ± 3	−878 ± 6	−6100 ± 5	−6880 ± 9	−2580 ± 28
Undersaturation experiments				−6100 ± 5	−6890 ± 10	−2650 ± 32
HNO_3	300 ± 2	–	–			
HCl	300 ± 3	40 ± 3	−879 ± 7			
H_2SO_4	299 ± 3	53 ± 9	−820 ± 30			
Calorimetric method [14]				−6090 ± 7	−6885 ± 8	−2667 ± 4

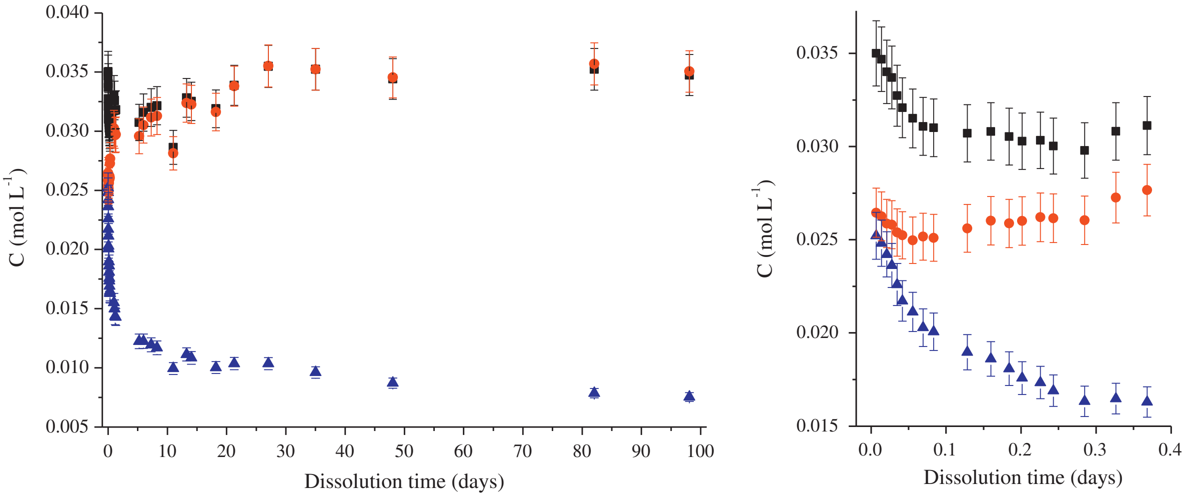

Fig. 7. Evolution of C_U(■), C_P(●) and C_{Cu} (▲) obtained during the dissolution of natural meta-torbernite in 1 mol L^{-1} HCl at 296 K (left) and focus on the early days of dissolution (right).

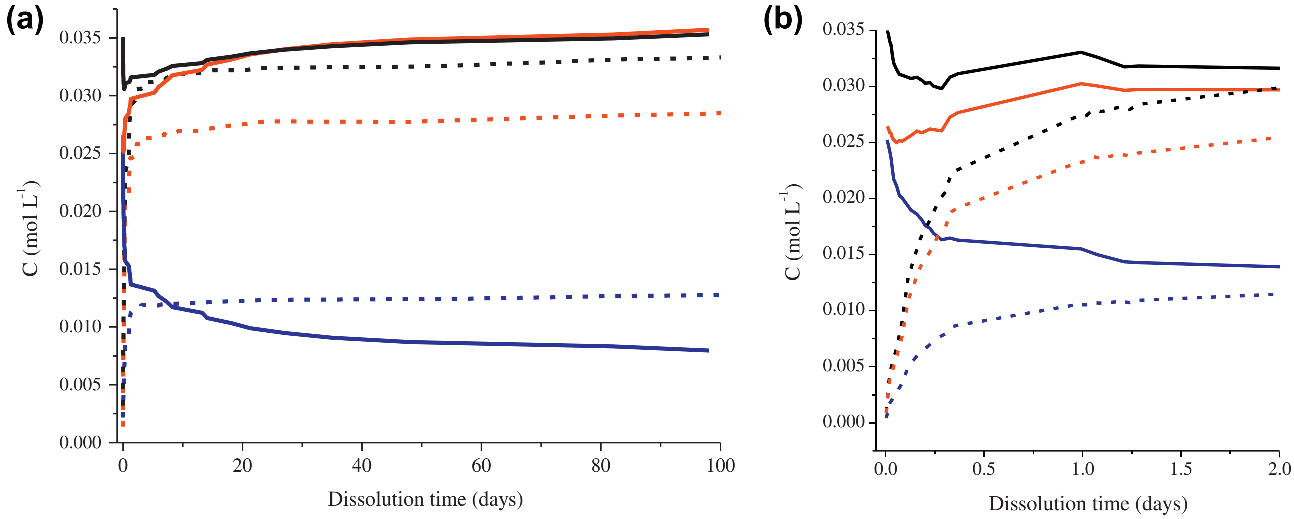

Fig. 8. Evolution of the elemental concentrations of U (black), P (red) and Cu (blue) for natural (solid lines) and synthetic (dash lines) meta-torbernite at 296 K in 1 mol L^{-1} HCl (a) and zoom on the early days of dissolution (b). (For interpretation of the references to color in this figure legend, the reader is referred to the web version of this article.)

Table 8
Elemental release rates and solubility constant related to natural meta-torbernite at 296 K. Comparison with values obtained for the synthetic sample.

		k(U) mol L^{-1} J^{-1}	k(P) mol L^{-1} J^{-1}	k(Cu) mol L^{-1} J^{-1}	$K^{\circ}_{s,0}$ (296 K)
Natural sample	HNO_3	2.1 ± 0.1	1.4 ± 0.1	3.1 ± 0.1	(2 ± 1) × 10^{-53}
	HCl	2.5 ± 0.1	1.9 ± 0.1	3.6 ± 0.1	(2 ± 1) × 10^{-53}
	H_2SO_4	6.0 ± 0.1	6.5 ± 0.1	6.0 ± 0.1	(4 ± 2) × 10^{-53}
Synthetic sample	HNO_3	0.03 ± 0.01	0.03 ± 0.01	0.029 ± 0.007	(1.0 ± 0.1) × 10^{-53}
	HCl	0.035 ± 0.005	0.030 ± 0.002	0.028 ± 0.001	(1.1 ± 0.5) × 10^{-53}
	H_2SO_4	0.039 ± 0.005	0.030 ± 0.005	0.031 ± 0.002	(1.9 ± 0.9) × 10^{-53}

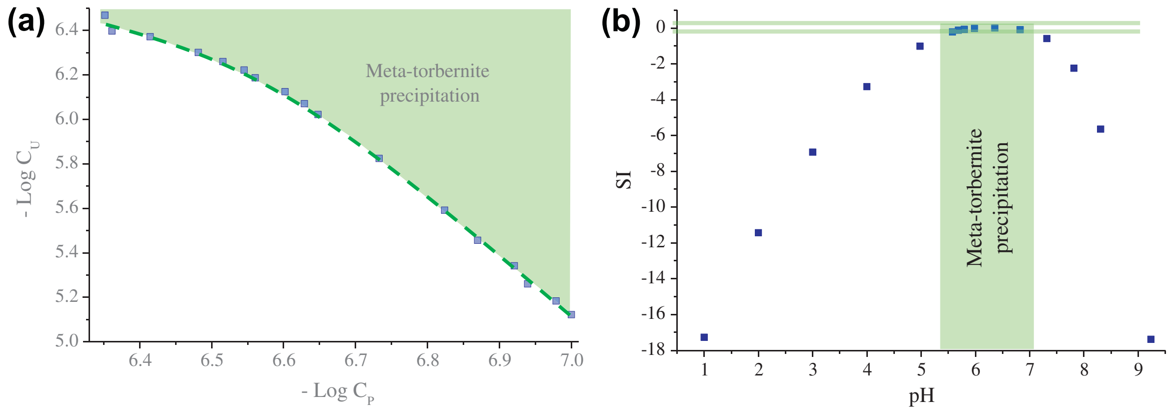

Fig. 9. (a) Range of precipitation of meta-torbernite (pH = 6.5 and Eh = 0.8 V/ENH) and (b) variation of the saturation index with regard to meta-torbernite precipitation versus the pH value (Eh = 0.8 V/ENH, $C_U = 4.2 \times 10^{-7}$ mol L^{-1}, $C_{Cu} = 1.6 \times 10^{-7}$ mol L^{-1}, and $C_P = 2.6 \times 10^{-7}$ mol L^{-1}).

(1.3 ± 0.4) × 10^{-53}) allowed us to evaluate uranium speciation under relevant conditions in the case of groundwater contamination (oxidative conditions, low temperature, low ionic strength and circumneutral pH).

For this purpose the influence of the uranyl ion and phosphoric acid concentration on meta-torbernite precipitation was examined in solution with a pH close to 6.5 (which corresponds to a pH commonly found in natural waters), oxidizing conditions with a redox potential *Eh* close to 0.8 V/NHE (equilibrium with O_2 and CO_2 of air) and a fixed concentration of copper (1.6 × 10^{-7} mol L^{-1}, less than the maximum recommended value (1.6 × 10^{-6} mol L^{-1}) for drinking water [43]). The solubility limit for meta-torbernite in terms of uranium and phosphorus elemental concentrations was then evaluated with PHREEQC-2 software (Fig. 9a) using thermodynamic data indicated in Table S1. Under these conditions, meta-torbernite was found to precipitate for $1 \times 10^{-7} < C_P < 4.5 \times 10^{-7}$ mol L^{-1} and $3.4 \times 10^{-7} < C_U < 7.6 \times 10^{-6}$ mol L^{-1}, concentrations typically found in mine water [44].

In addition, the influence of pH on the stability of meta-torbernite (SI[1]) was also examined for uranium, copper, and phosphorus concentrations of $C_U = 4.2 \times 10^{-7}$ mol L^{-1}, $C_{Cu} = 1.6 \times 10^{-7}$ mol L^{-1},

---

[1] $\mathrm{SI} = \log(\frac{Q}{K_s})$ with $Q = \prod_i (a_i)^{\nu_i}$ where ν_i is the stoichiometric coefficient (algebraic value) of species i and a_i the nonequilibrium activity of i.

and $C_P = 2.6 \times 10^{-7}$ mol L^{-1}, respectively (Fig. 9b). From these results, meta-torbernite precipitated at $5.5 \leqslant pH \leqslant 7$ (which is the typical value obtained in most of groundwater [43]).

These results highlight that meta-torbernite can easily precipitate in the vicinity of uranium mines where phosphate and copper are also encountered. In this simulation, a simplified system was considered. However, considering natural systems makes more complex the prediction of the behavior of uranyl. Indeed, the presence of other elements like Si, Ca, Mg or K may affect the precipitation of the meta torbernite. Such site-specific simulations were not performed as they require an accurate knowledge of the water composition.

4. Conclusion

The solubility properties of meta-torbernite, $(H_3O)_{0.4}Cu_{0.8}(UO_2)_2(PO_4)_2 \cdot 7.6H_2O$, were studied in various operating conditions, including experiments under- and supersaturated conditions, respectively for the both synthetic and natural samples. The complex composition of natural meta-torbernite evidenced the need to prepare pure single-phase samples since the separation from the host rock failed to eliminate all the impurities. In this context, the method of preparation developed here allowed the precipitation of pure meta-torbernite exhibiting morphology and chemical composition close to that of the natural sample.

On the basis of obtained values during the dissolution tests, the experiments in supersaturated conditions allowed us to determine reliable values of $\log K^{\circ}_{s,0}(298\text{ K}) = -52.9 \pm 0.1$ and of associated thermodynamic data: $\Delta_R G^{\circ}(298\text{ K}) = 300 \pm 2$ kJ mol^{-1}; $\Delta_R H^{\circ}(298\text{ K}) = 40 \pm 3$ kJ mol^{-1}, and $\Delta_R S^{\circ}(298\text{ K}) = -879 \pm 7$ J mol^{-1} K^{-1}. These values were found to be in good agreement with those previously reported from calorimetric measurements which confirmed that the approach to equilibrium from under- and supersaturated conditions developed in this study can provide reliable thermodynamic data. The preparation of synthetic samples thus appeared as an easy way to study the solubility properties of meta-torbernite.

In addition, the dissolution tests performed on natural samples allowed us to consolidate the values obtained for the solubility constant. Indeed, although the kinetics differ strongly from the synthetic compounds, probably because of self-irradiation and the presence of impurities, a similar steady state was achieved. Thus, working with natural samples in solubility experiments requires a careful pretreatment in order to obtain pure and stoichiometric phase. However, it is of great interest in order to understand groundwater interactions with site-specific meta-torbernite bearing rocks, sediments and soils, providing that all the phases are identified in the phase assembly and that all cations and anions are considered in the speciation model taking into account most of the potential reaction equilibria.

Finally, the data determined experimentally were also used to estimate the conditions of meta-torbernite precipitation in environmental media similar to those encountered in former mining sites. From these calculations, meta-torbernite formation appeared to partly control the concentration of uranium in the underground water considered, and thus its migration to the geosphere. In order to predict more accurately the long-term behavior of uranium in such sites, it now appears necessary to study the formation of additional phases of interest, mainly composed by uranyl phosphates and/or vanadates. Studies are currently in progress to determine thermodynamic data related to several phases of interest, including meta-autunite ($Ca(UO_2)_2(PO_4)_2 \cdot 6H_2O$), ankoleite ($K_2(UO_2)_2(PO_4)_2 \cdot 6H_2O$) or carnotite ($K_2(UO_2)_2(VO_4)_2 \cdot 3H_2O$), and will be published soon.

Acknowledgements

This work was kindly supported by the PACEN GUTEC (Geology of Uranium and Thorium: Extraction, Conversion), NEEDS Ressources (mines, processes, economy) projects of the CNRS and the NOPRA (Nouveaux Procédés pour l’Amont) program of the CEA. The authors are grateful to Prof. Francis Abraham (Laboratory of Catalysis and Solid State Chemistry, ENSCL) for very fruitful and valuable discussions regarding our results, to Johann Ravaux (Laboratory of Environmental Microscopy, ICSM) for the ESEM and X-EDS analyses and to Veronique Dubois (Laboratory of Ion Separation using Molecular self-assembled colloids, ICSM) for the ICP-AES analyses.

Appendix A. Supplementary material

Supplementary data associated with this article can be found, in the online version, at http://dx.doi.org/10.1016/j.jnucmat.2013.08.037.

References

[1] J.E. Stubbs, J.E. Post, D.C. Elbert, P.J. Heaney, D.R. Veblen, Am. Mineral. 95 (2010) 1132–1140.
[2] R. Finch, T. Murakami, Rev. Miner. 38 (1999) 91–179.
[3] M. Cuney, K. Kyser, Recent and not-so-Recent Developments in Uranium Deposits and Implications for Exploration, vol. 39, Mineralogical Association of Canada, Quebec city, 2008.
[4] International Atomic Energy Agency, Safety Reports Series No. 78, Radiation Protection And Management of NORM Residues in the Phosphate Industry, 2013.
[5] T. Murakami, T. Ohnuki, H. Isobe, T. Sato, Am. Mineral. 82 (1997) 888–899.
[6] L. Galoisy, M. Gérard, T. Poquet, G. Calas, M. Descostes, V. Phrommavanh, Supergene evolution of granitic waste rock piles around U-mines in the Saint-Sylvestre Area (French Massif Central), Goldschmidt Conference, Montreal, Canada, 24-29 June 2012.
[7] R. Vochten, P. Piret, A. Goeminne, Bull. Mineral. 104 (1981) 457–467.
[8] F.J. Dahlkamp, Uranium Deposits of the World – USA and Latin America, Eds Springer, Germany, 2010.
[9] F.J. Dahlkamp, Uranium Deposits of the World – Asia, Eds Springer, Germany, 2009.
[10] T. Hedman, A. Nystrom, C. Thegerstrom, C. R. Phys. 3 (2002) 903–913.
[11] R. Rosborg, L. Werme, J. Nucl. Mater. 379 (2008) 142–153.
[12] R. Guillaumont, T. Fanghanel, V. Neck, J. Fuger, D.A. Palmer, I. Grenthe, M.H. Rand, Update on the chemicals Thermodynamics of uranium, Neptunium, Plutonium, Americium and Technetium, vol. 5, North Holland Elsevier Science Publishers B.V, Amsterdam, The Netherlands, 2003.
[13] V. Pekarek, V. Vesely, J. Ullrich, Bull. Soc. Chim. France 27 (1968) 1844–1847.
[14] N.V. Karyakin, N.G. Chernorukov, E.V. Suleimanov, O.A. Egorova, M.I. Alimzhanov, S.A. Gavrilova, RadioChemistry 44 (2002) 219–223.
[15] E.S. Ilton, J.M. Zachara, D.A. Moore, J.P. Mckinley, A.D. Eckberg, C.L. Cahill, A.R. Felmy, Environ. Sci. Technol. 44 (2010) 7521–7526.
[16] N. Dacheux, V. Brandel, M. Genet, New J. Chem. 19 (1995) 1029–1036.
[17] K.A. Hughes Kubatko, K.B. Helean, A. Navrotsky, P.C. Burns, Science 132 (2003) 1191–1193.
[18] N. Dacheux, J. Aupiais, Anal. Chem. 69 (1997) 2275–2282.
[19] R. Berman, Am. Mineral. 42 (1957) 905–908.
[20] T. Roisnel, J. Rodriguez-Carvajal, Mater. Sci. Forum. 378–381 (2001) 118–123.
[21] N. Dacheux, J.F. Le Dû, V. Brandel, M. Genet, New J. Chem. 20 (1996) 507–514.
[22] D.L. Parkhurst, C.A.J. Appelo, User’s guide to PHREEQC (Version2) – A Computer Program Forspeciation, Batch-reaction, one-Dimensional Transport, and Inversegeochemical Calculations, U.S.G.S. Water-Resources Investigations, Report 99-4259, 1999.
[23] J.D. Allison, D.S. Brown, K.J. Novo-Grada, MINTEQA2/PRODEFA2 – A Geochemical Assessment Model for Environmental Systems – Version 3.0 User’s Manual: Environmental Research Laboratory, Office of Research Athens, Georgia, 1990.
[24] I. Grenthe, B. Lagerman, Radiochim. Acta 61 (1993) 169–176.
[25] T. Vercouter, B. Amekraz, C. Moulin, E. Giffaut, P. Vitorge, Inorg. Chem. 44 (2005) 7570–7581.
[26] R. Silva, G. Bidoglio, M. Rand, P. Robouch, H. Wanner, I. Puigdomenech, Chemical Thermodynamics of Americium, vol. 2, North Holland Elsevier Science Publishers B.V, Amsterdam, The Netherlands, 1995.
[27] R. Lemire, J. Fuger, H. Nitsche, M. Rand, K. Spahiu, J. Sullivan, W. Ullman, P. Vitorge, Chemical Thermodynamics of Neptunium and Plutonium, vol. 4, North Holland Elsevier Science Publishers B.V, Amsterdam, The Netherlands, 2001.
[28] A.J. Locock, P.C. Burns, Can. mineral. 41 (2003) 489–502.
[29] W.T.F. Barth, Am. J. Sci. 23 (1993) 350–356.

[30] J. Bennett, R. Kirchner, Zeolites 12 (1992) 338–342.
[31] D.M. Wellman, J.P. Icenhower, A.P. Gamerdinger, S.W. Forrester, Am. Mineral. 91 (2006) 143–158.
[32] N. Dacheux, N. Clavier, J. Ritt, J. Nucl. Mater. 349 (2006) 291–303.
[33] N.M. Rose, Geochim. Cosmochim. Acta 55 (1991) 3273–3286.
[34] J. Ganor, J.L. Mogollon, A.C. Lasaga, Geochim. Cosmochim. Acta 59 (1995) 1037–1052.
[35] W.H. Casey, M.F. Hochella, H.R. Westrich, Geochim. Cosmochim. Acta 57 (1993) 785–793.
[36] S. Hubert, G. Heisbourg, N. Dacheux, P. Moisy, Inorg. Chem. 47 (2008) 2064–2073.
[37] N. Dacheux, E. Du Fou de Kerdaniel, N. Clavier, R. Podor, J. Aupiais, S. Szenknect, J. Nucl. Mater. 404 (2010) 33–43.
[38] D. Gorman-Lewis, T. Shvareva, K.A. Kubatko, P.C. Burns, D.M. Wellman, B. Mcnamara, J.E.S. Szymanowski, A. Navrotsky, J.B. Fein, Environ. Sci. Technol. 43 (2009) 7416–7422.
[39] B.E. Burakov, M.A. Yagovkina, V.M. Garbuzov, A.A. Kitsay, V.A. Zirlin, Mater. Res. Soc. Symp. Proc. 824 (2004) 219–223.
[40] X. Deschanels, V. Picot, B. Glorieux, F. Jorion, S. Peuget, D. Roudil, C. Jegou, V. Broudic, J.N. Cachia, T. Advocat, C. Den Auwer, C. Fillet, J.P. Coutures, C. Hennig, A.J. Scheinost, Nucl. Mater. 352 (2006) 233–240.
[41] C. Tamain, A. Ozgumus, N. Dacheux, F. Garrido, L.J. Thomé, Nucl. Mater. 352 (2006) 217–223.
[42] R. Roy, E.R. Vance, J. Mater. Sci. 16 (1981) 1190–1197.
[43] C.A.J. Appelo, D. Postma, Geochemistry, Groundwater and Pollution, A.A. Balkema, Rotterdam, Netherlands, 1996.
[44] AREVA. Bilan décennal environnemental de la Crouzille 1994–2003. Rapport Etablissement de Bessines, 2003.